Phase Transition on Si(001) and Silicide Formation in Au-Si Interface

シリコン清浄表面の相転移および金-シリコン界面でのシリサイド形成の研究

Masakazu Kubota

窪田昌一

(1)

Phase Transition on Si(001)
and
Silicide Formation in Au-Si Interface

Masakazu Kubota

ACKNOWLEDGMENTS

I am very grateful to Prof. Y. Murata for his good direction and stimulating discussion in this work. Through the discussion I have learned many things, e. g. mental attitudes for performing a research. I am thankful to collaborator: Prof. M. Iwami, Prof. H. Tochihara, Dr. T. Aruga, Mr. T. Tabata, Mr. T. Koyama, and Mr. T. Terada for their kind instruction and support. I am also thankful for many fruitful discussion with Prof. A. Yoshimori, Prof. K. Tanaka, Prof. K. Terakura, Prof. T. Kawamura, and Dr. K. Kakitani. Hospitalities of Computing Center and Synchrotron Radiation Laboratory of the Institute for Solid State Physics at the University of Tokyo are acknowledged.

CONTENTS

Chapter 1

General introduction

Silicon is a typical substance in semiconductors and the most important material for electronics devices. Hence, the bulk properties have been extensively studied for practical importance and fundamental interest.[1,2] Silicon surfaces have been also extensively studied. Silicon-metal interfaces are also important for device technology and the structure of silicide formation has been discussed. Consequently, many useful results for electronics devices have been obtained and many important properties for scientific research have been elucidated. However, simple unresolved problems remain in the fundamental field, e.g. phase transitions appearing at low-index surfaces and the reaction mechanism in silicide formation. These problems are closely correlated with the bond nature of silicon-silicon and silicon-metal.

The covalent bond in silicon forms a strong directional bond. However, new bondings are produced at surfaces and interfaces, and then, bond angle is deformed within a restricted variation of bond length. In order to reduce number of surface dangling bonds, it is necessary for surface atoms to change the bond nature, where atoms of second and/or third layers displace from a bulk position. A competition between electronic energy and elastic strain determines the surface structure in a reconstruction, and reconstructions are observed at most of the clean surfaces of covalent-bond crystals. There show different reconstruction structures in the different-index surfaces.

Schlier and Farnsworth[3] first reported in 1959 that a low-energy

electron diffraction (LEED) pattern on the annealed Si(111) surface shows a 7×7 structure. Many scientists studied for a long time this surface using various techniques and accumulated structural information.[4] A dimer, adatom, and stacking-fault (DAS) model was finally proposed by Takayanagi et al.[5] through transmission electron diffraction (TED) observations of Si(111)-7×7. Scanning tunneling microscopy (STM) measurements[6,7] with different bias voltages support the DAS model. Other various results[8,9] also support this model and the structure of Si(111)-7×7 has been settled.

On the contrary, the structure of the clean Si(001) surface has been confused. Schlier and Farnsworth[3] also reported that a LEED pattern on Si(001) show a 2×1 structure consisting of two orthogonal domains along the [110] and [$\bar{1}$10] directions. They proposed a dimer model pairing the topmost two atoms to reduce two dangling-bonds of each atom to one. Lander and Morrison[10] observed quater-order LEED spots showing a c(4×2) pattern, and explained that the dimer and the two-atom vacancy order alternatively at the surface. After that, most of scientists observed only the 2×1 structure as the clean surface and studied using various techniques, and then the problem on the 2×1 local configuration happened.[11-14] An asymmetric dimer model for the local configuration was proposed from theoretical consideration[15-21] and supported by several experimental results, LEED,[22,23] ARUPS,[24-26] core shift,[27] ISS,[28-30] $\Delta\phi$,[31] reflectance,[32] and EELS.[33] However, the asymmetric dimer model were doubted with aid of the recent STM measurement.[34,35]

Five groups[10,38-39] have observed the c(4×2) structure by using LEED or helium diffraction. Murata's group[38] found a phase transition from 2×1 to c(4×2) at 200 K on Si(001) as well as on Ge(001) found by Kevan et al.[40] When the asymmetric dimer configuration is employed in the ordered c(4×2) structure, the 2×1 structure can be explained as a disordered arrangement of the asymmetric dimers.

I shall take up this problem correlated with the phase transition and describe the detailed observations of a streak pattern well above the transition temperature in chapter 3. The phase transition is closely related to the nature of the surface bonds generated for reducing the dangling bond density and the backbonds. For the detailed observations of the streak pattern, I have developed a rapid measuring system of LEED patterns by using a video camera. I shall mention this system in chapter 2.

I shall also describe room-temperature-alloyed interface formation (RTAIF) with gold deposited on silicon in chapter 4. Although this phenomenon was found in an application field,[41] important problems for fundamental research happen. In the case of silver deposition on silicon, no alloy formation takes place.[42] The common sense in chemistry implies that gold has much lower reactivity with silicon than silver. The above result is clearly contradictory. I have carried out photoemission measurements using synchrotron radiation in order to elucidate the mechanism of gold-silicon alloy formation. When gold atoms are adsorbed on silicon

surfaces, a covalent-like bond is formed between a surface silicon and a gold atom and a backbond of the surface silicon atom is weakened. Next, the metallic phase appears with higher gold coverage. For RTAIF, the covalent-like bond formation is essentially important.

REFERENCES

[1]K. Seeger, *Semiconductor Physics-An Introduction*, 2nd ed. (Springer-Verlag, Berlin, 1982).

[2]S. M. Sze, *Physics of Semiconductor Devices*, 2nd ed. (John-Wiley, New York, 1981).

[3]R. E. Schlier and H. E. Farnsworth, J. Chem. Phys. 30, 917 (1959).

[4]See for example *ref. 5*

[5]K. Takayanagi, Y. Tanishiro, M. Takahashi, and S. Takahashi, J. Vac. Sci. Technol. A 3, 1502 (1985); K. Takayanagi, Y. Tanishiro, S. Takahashi, and M. Takahashi, Surf. Sci. 164, 367 (1985).

[6]R. S. Becker, J. A. Golovchenko, E. G. McRae, and B. S. Swartzentruber, Phys. Rev. Lett. 55, 2028 (1985).

[7]R. M. Tromp, R. J. Hamers, and J. E. Demuth, Phys. Rev. B 34, 1388 (1986); R. J. Hamers, R. M. Tromp, and J. E. Demuth, Phys. Rev. Lett. 56, 1972 (1986).

[8]I. K. Robinson, W. K. Waskiewicz, P. H. Fuoss, J. B. Stark, and P. A. Bennett, Phys. Rev. B 33, 7013 (1986).

[9]R. M. Tromp and E. J. van Loenen, Surf. Sci. 155, 441 (1985).

[10]J. J. Lander and J. Morrison, J. Appl. Phys. 33, 2088 (1962); J. J. Lander and J. Morrison, J. Chem. Phys. 37, 729 (1962).

[11]J. E. Rowe and H. Ibach, Phys. Rev. Lett. 31, 102 (1973).

[12]J. E. Rowe and H. Ibach, Phys. Rev. Lett. 32, 421 (1974).

[13]F. Jona, H. D. Shih, A. Ignatiev, D. W. Jepsen, and P. M. Marcus, J. Phys. C 10, L67 (1977).

[14]J. A. Appelbaum, G. A. Baraff, and D. R. Hamann, Phys. Rev. Lett. 35, 729 (1975).

[15]J. A. Appelbaum and D. R. Hamann, Surf. Sci. 74, 21 (1978).

[16]D. J. Chadi, Phys. Rev. Lett. 43, 43 (1979).

[17]J. Ihm, M. L. Cohen, and D. J. Chadi, Phys. Rev. B 21, 4592 (1980).

[18]W. S. Verwoerd, Surf. Sci. 99, 581 (1980).

[19]M. T. Yin and M. L. Cohen, Phys. Rev. B 24, 2303 (1981).

[20]M. A. Bowen, J. D. Dow, and R. E. Allen, Phys. Rev. B 26, 7083 (1982).

[21]A. Mazur and J. Pollmann, Phys. Rev. B 26, 7086 (1982).

[22]W. S. Yang, F. Jona, and P. M. Marcus, Solid State Commun. 43, 847 (1982); W. S. Yang, F. Jona, and P. M. Marcus, Phys. Rev. B 28, 2049 (1983).

[23]S. J. White, D. C. Frost, and K. A. R. Mitchell, Solid State Commun. 42, 763 (1982).

[24]F. J. Himpsel and D. E. Eastman, J. Vac. Sci. Technol. 16, 1297 (1979).

[25]H. A. van Hoof and M. J. van der Wiel, Appl. Surf. Sci. 6, 444 (1980).

[26]R. I. G. Uhrberg, G. V. Hansson, J. M. Nicholls, and S. A. Flodström, Phys. Rev. B 24, 4684 (1981).

[27]F. J. Himpsel, P. Heimann, T. -C. Chiang, and D. E. Eastman, Phys. Rev. Lett. 45, 1112 (1980).

[28]M. Aono, Y. Hou, C. Oshima, and Y. Ishizawa, Phys. Rev. Lett. 49, 567 (1982).

[29]R. M. Tromp, R. G. Smeenk, and F. W. Saris, Surf. Sci. 133, 137 (1983).

[30]L. C. Feldman, P. J. Silverman, and I. Stensgaard, Nucl. Instrum. Methods 168, 589 (1980).

[31]P. Koke and W. Mönch, Solid State Commun. 36, 1007 (1980).

[32]P. E. Wierenga, M. J. Sparnaay, and A. van Silfhout, Surf. Sci. 99, 59 (1980).

[33]H. H. Farrell, F. Stucki, J. Anderson, D. J. Frankel, G. J. Lapeyre, and M. Levinson, Phys. Rev. B 30, 721 (1984).

[34]R. M. Tromp, R. J. Hamers, and J. E. Demuth, Phys. Rev. Lett. 55, 1303 (1985); R. J. Hamers, R. M. Tromp, and J. E. Demuth, Phys. Rev. B 34, 5345 (1986).

[35]R. J. Hamers, Ph. Avouris, and F. Bozso, Phys. Rev. Lett. 59, 2071 (1987).

[36]T. D. Poppendieck, T. C. Ngoc, and M. B. Webb, Surf. Sci. 75, 287 (1978).

[37]K. Müller, E. Lang, L. Hammer, W. Grimm, P. Heilmann, and K. Heinz, *Determination of Surface Structure by LEED*, ed. by P. M. Marcus and F. Jona (Plenum, New York, 1984).

[38]T. Tabata, T. Aruga, and Y. Murata, Surf. Sci. 179, L63 (1987).

[39]M. J. Cardillo and G. E. Becker, Phys. Rev. Lett. 40, 1148 (1978); M. J. Cardillo and G. E. Becker, Phys. Rev. B 21, 1497 (1980); A. Sakai, M. J. Cardillo, and D. R. Hamann, Phys. Rev. B 33, 5774 (1986).

[40]S. D. Kevan and N. G. Stoffel, Phys. Rev. Lett. 53, 702 (1984); S. D. Kevan, Phys. Rev. B 32, 2344 (1985).

[41]A. Hiraki, M. A. Nicolet, and J. W. Mayer, Appl. Phys. Lett. 18, 178 (1971); A. Hiraki, Surf. Sci. Rep. 3, 357 (1984).

[42]G. Le Lay, Surf. Sci. 132, 169 (1983); and references therein.

Chapter 2

Rapid measuring system of LEED

2.1. INTRODUCTION

Three-dimensional periodicity of crystals is truncated at surfaces, so that bondings characteristic of the surface are formed. The electronic structure and the atomic geometry at the surface reflect the bonding nature and show interesting behavior.[1] Hence, knowledge of the surface geometry is very important for understanding surface properties. The surface structures have been studied by various methods.[2] In particilar, the LEED method has been used for determination of many stable ordered structures in conjunction with dynamical calculation.[3-5] In the LEED experiment for structure analysis, diffracted-beam intensities along reciprocal rods are measured as a function of incident electron energy, i.e. I-V curves. A few techniques have been developed for measuring the I-V curve. A Faraday cup detector was used in an early work.[6,7] Spotphotometry,[8] photographic film,[9] and video photography[10-18] have been applied to the intensity measurements of diffraction spots on a phospher screen.

The structural phase transition can be observed at crystal surfaces and adsorbate layers with temperature change and/or coverage change of the adsorbate. Recently, the study of these dynamical features in structures has been advanced.[19-21] In order to study these phenomena by using LEED, it is necessary to analyze, in addition to the diffraction beam profiles, diffuse-scattering patterns showing short-range ordering or the domain structure. Then, the detection system with a large dynamic range is required to detect

scattered electrons in a wide angular range at the same time. A display type LEED apparatus is useful for this purpose.

Several groups constructed a conventional LEED apparatus using a video camera in order to convert light into analog electric signal. On the other hand, Stair[22] and McRae et al.[23] made a new type LEED intensity measurement system using a position sensitive detector (PSD), which replaces the phospher screen in a conventional LEED optics in order to detect scattered electrons directly and to connect an electric signal. In both the camera and the PSD technique, analog signal data are digitized in a frame memory and are saved into a computer memory system. The advantage of this method is an easy performance of a rapid intensity measurements and quick analysis.

A video camera acquisition system can be applied to other display type measurement systems, e.g. another LEED or reflection high-energy electron diffraction (RHEED). I have constructed a rapid measuring system to study dynamical behavior of surface structures.

2.2. DATA HANDLING

The data acquisition system is shown schematically in Fig. 1. Thick arrows represent data streams connecting block. Thin arrows represent signals controlling each block from a micro-computer and vertical synchronized pulse train which is a time base of this whole system.

Two modes are available for the data acquisition in this system. First is an off-line mode, in which data from a video camera are recorded in a video disk or a tape recorder, and then the recorded data are sent through a frame memory, in which the analog data are digitized, into an analyzing computer, i.e. a micro- or a host computer. This mode can record the video data in a high acquisition rate for a long time, for which the storage capacity of the video tape recorder is available. When an acquisition time is given priority, this mode is used.

Second is an on-line mode, in which the video data are directly sent to a host computer without recording in an analog recorder and are saved into the computer memory system. In this mode, the best experimental condition can be easily arranged with the feedback system, in which the observed pattern is immediately analyzed and the required condition such as symmetry of the diffraction pattern is examined, and the digitized data can be stored for a long time without distortion.

2.3. DETAILS OF EQUIPMENT

A conventional, four grid and phospher screen type, LEED optics (Varian, 981-0127) and an electron gun/controller (Varian, 981-2125) are installed in a ultra high vacuum (UHV) apparatus. The gun system contains a filament assembly which is mounted at angle 13° off the

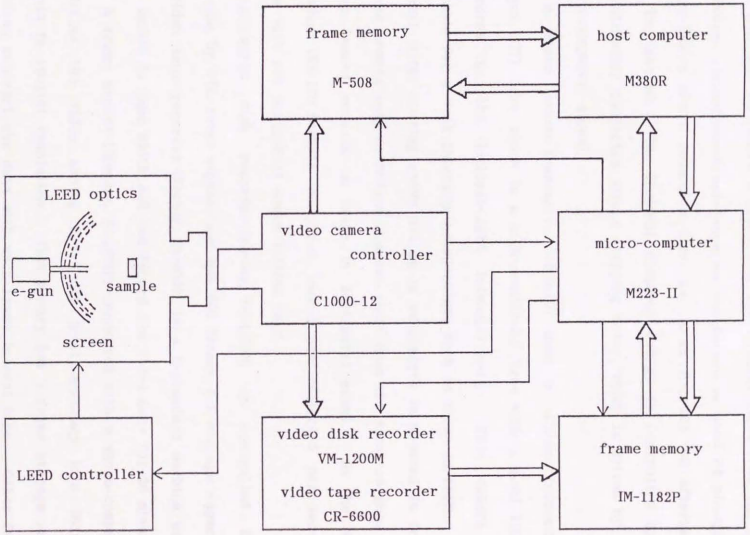

FIG. 1. Block diagram of rapid measuring LEED system.

main gun axis to reduce a leakage of the filament light from the exit aperture. Fluorescent substance on the screen is used P4 phospher, which has a short reduction time, i.e. 30 μs for 10%, so afterimage can be ignored. The incident electron energy is controlled by a potentiometer connected with a stepping motor, which is driven by the micro-computer signal.

A video camera (Hamamatsu, C1000-12) uses a silicon intensifier target (SIT) tube, which is a high-sensitivity tube with a good linear response to the incident-light intensity (γ=1). This camera is suitable for a weak intensity measurements such as those in LEED. An optical filter cutting above 570 nm in wavelength is mounted in front of the camera lens to reduce filament light from the electron gun. The video camera records an image in horizontal scans. In the NTSC standard (RS-170 format), 30 video images are collected per second, each with 480 horizontal scans lasting 64μs.

A video disk recorder (Victor, VM-1200M) is controlled from outside by TTL level signals and has 600 frames for storage capacity. A video tape recorder (Victor, CR-6600) is a U-standard machine using 3/4 inches in tape width and can record the video data for 20 minutes.

A frame memory (Ikegami, IM-1182P) connected with a micro-computer digitizes the video analog data with 8-bit accuracy into 768×512 pixels in spatial resolution. This memory has 2 frame storage areas and can subtract the data with each frame in real time. Other frame memory(Graphica, M-508) connected with the host computer also degitizes the analog video picture with 8-bit into 512×512 pixels.

When the wide area data are accumulated or analyzed, this data handling system is useful since the throughput of this system is much faster than that with the former frame memory. Two video monitors are always used for display of both the camera output and the digitized image from the frame memory.

A micro-computer (Sord, M223-II), 8-bit CPU machine, is used as a controller for each block and is sometimes used for analyzing the data when the data are not so many. The operating system (OS) of this computer is supplied by an original disk-operating system (DOS) from Sord company. Available programing languages are assembly, Fortran, and BASIC on this OS. The measuring programs were made by using an assembly as a low-level driver for controlling each block and by using a Fortran as a top-level program for calling these drivers. Among these languages a particular one was selected so as to make the execution speed fastest. In the data transfer from and to the host computer, a serial communication, RS-232C, is used at 2400 bits per second. A host computer(FACOM, M380R) is used for the data storage and/or analysis. Contour maps, bird's-eye views, and spot profiles are easily obtained.

In I-V curve measurement, maximum acquisition rate in the off-line mode is determined by the period of video synchronized signal and frame blanking. Usually, frame blanking is not used, so the maximum rate is 1/15 second, which is twice of synchronized period. Two or three hundreds diffraction images from 30 to 300 eV for primary electron energy can be obtained in 20 seconds.

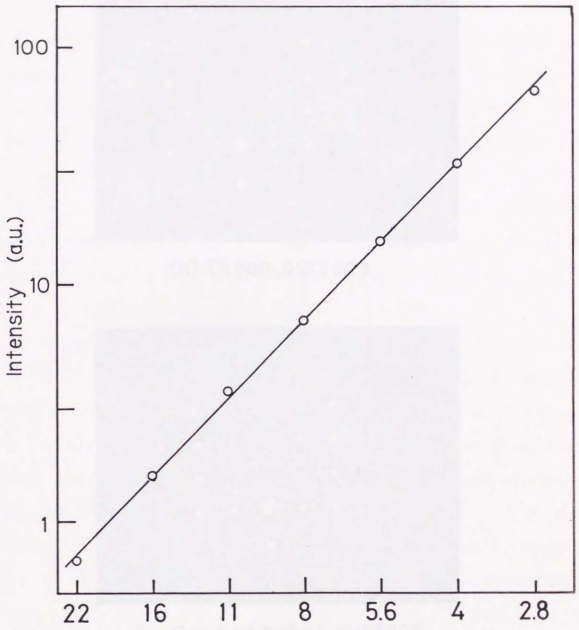

FIG. 2. Digitized data vs exposure of incident light.

Si(001)-c(4×2)

Ep = 53 eV, T = 100 K, p = 6×10^{-11} torr

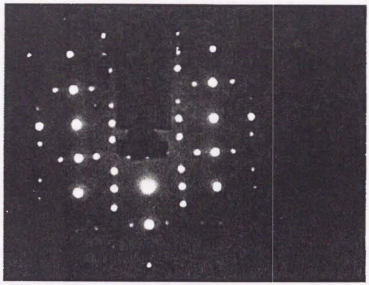

(a) Clean surface

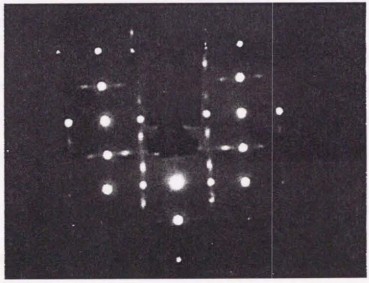

(b) Contaminated surface

FIG. 3. LEED patterns on Si(001)-c(4×2) surfaces at low temperature.
(a):Immediately after cleaning
(b):After thirty minutes from (a) in 6×10^{-11} torr

2.4. PERFORMANCE

In order to examine the total linearity of this system, I have measured the relation between light intensity and digitized data without accumulation. The result is shown in Fig. 2. These observed points are obtained after background subtraction. The dynamic range has 2-order magnitude. When N frames are accumulated, the dynamic range is expanded into $\sqrt{N}$ times this amount. Hence, this method is effective to get a good signal-to-noise ratio for a low-intensity image accompanied with diffraction spots of high intensity such as a diffuse and a streak pattern.

Figures 3(a) and 3(b) show LEED patterns of the Si(001) surface immediately after cleaning and of the contaminated one at thirty minutes later in 6×10^{-11} torr, respectively. The quarter order spots are obviously changed into a streaky pattern by contamination even in this good vacuum. Hence, the rapid intensity measurement is important for avoiding the contamination effect. This rapid measuring system is valid not only for studing dynamical phenomena like a phase transition but also for studing the specimen which is very easily contaminated by residual gases. Phase transition on this clean surface will be described in chapter 3.

The LEED observations using this measuring system give us several new important results cocerning dynamical behaviors in the surface structure.[24-28]

REFERENCES

[1]for example: R. Imbihl, M. P. Cox, and G. Ertl, J. Chem. Phys. 84, 3519 (1986).

[2]M. A. Van Hove and S. Y. Tong, *The Structure of Surfaces*, (Springer-Verlag, Berlin, 1985).

[3]J. B. Pendry, *Low Energy Electron Diffraction*, (Academic press, London, 1974).

[4]M. A. Van Hove and S. Y. Tong, *Surface Crystallography by LEED*, (Springer-Verlag, Berlin, 1979).

[5]M. A. Van Hove, W. H. Weinberg, and C. -M. Chan, *Low-Energy Electron Diffraction*, (Springer-Verlag, Berlin, 1986).

[6]C. J. Davisson and L.H. Germer, Phys. Rev. 30, 705 (1927).

[7]H. E. Farnsworth, Phys. Rev. 34, 679 (1929).

[8]F. Jona, Discuss. Faraday Soc. 60, 210 (1975).

[9]P. C. Stair, T. J. Kaminska, L. L. Kesmodel, and G. A. Somorjai, Phys. Rev. B 11, 623 (1975).

[10]P. Heilmann, E. Lang, K. Heinz, and K. Müller, Appl. Phys. 9, 247 (1976) ; E. Lang, P. Heilmann, G. Hanke, K. Heinz, and K. Müller, Appl. Phys. 19, 287 (1979).

[11]D. C. Frost, K. A. R. Mitchell, F. R. Shephend, and P. R. Watson, J. Vac. Sci. Technol. 13, 1196 (1976).

[12]T. N. Tommet, G. B. Olszewski, P. A. Chadwick, and S. L. Bernasek, Rev. Sci. Instrum. 50, 147 (1979).

[13]D. G. Welkie and M. G. Lagally, Appl. Surf. Sci. 3, 272 (1979).

[14]S. P. Weeks, J. E. Rowe, S. B. Chirstman, and E. E. Chaban, Rev. Sci. Instrum. 50, 1249 (1979).

[15]H. Leonhard, A. Gutmann, and K. Hayek, J. Phys. E: Sci. Instrum. 13, 298 (1980).

[16]V. E. de Carvalho, M. W. Cook, P. G. Cowell, O. S. Heavens, M. Prutton, and S. P. Tear, Vacuum 34, 893 (1984).

[17]J. W. Anderegg and P. A. Thiel, J. Vac. Sci. Technol. A 4, 1367 (1986).

[18]D. F. Ogletree and G. A. Somorjai, Rev. Sci. Instrum. 57, 3012 (1986).

[19]S. K. Sinha, *Ordering in Two Dimensions*, (North Holland, Amsterdam, 1980).

[20]T. L. Einstein, in *Chemistry and Physics of Solid Surfaces* IV, ed. by R. Vanselow and R. Howe, (Springer Verlag, Berlin, 1982).

[21]R. F. Willis, in *Dynamical Phenomena at Surfaces, Interfaces and Superlattices*, ed. by F. Nizzoli, K. -H. Rieder, and R. F. Willis, (Springer Verlag, Berlin, 1985).

[22]P. C. Stair, Rev. Sci. Instrum. 51, 132 (1980).

[23]E. G. McRae, R. A. Malic, and D. A. Kapilow, Rev. Sci. Instrum. 56, 2077 (1985).

[24]T. Aruga, H. Tochihara, and Y. Murata, Surf. Sci. 158, 490(1985).

[25]T. Tabata, T. Aruga, and Y. Murata, Surf. Sci. 179, L63 (1987) ; M. Kubota and Y. murata, submitted to Phys. Rev. B.

[28]M. Okada, H. Tochihara, and Y. Murata, Phys. Rev. B 43, 1411 (1991).

Chapter 3

Study of streak patterns in low-energy electron diffraction on Si(001)

3.1. INTRODUCTION

The clean Si(001) surface is one of the simplest reconstructed surfaces. This surface consists of the dimer row which is observed by scanning tunneling microscopy (STM)[1] and shows a phase transition between a 2×1 structure at room temperature and a c(4×2) structure at low temperatures.[2] This phase transition occurs at 200 K and can be represented by a second-order order-disorder transition.[2] The appearance of the c(4×2) structure implies that the Si(001) surface is described by the asymmetric configuration for the dimers, since the symmetric configuration is impossible to show a clear c(4×2) LEED pattern. Although the stable configuration is the p(2×2) structure, this phase transition was theoretically predicted by Ihm et al.[3] and simulated by a Monte Carlo method by Saxena et al.[4] on the basis of the asymmetric dimer model.

However, the asymmetric dimers for the stable configuration are doubted by the recent STM measurements. The symmetric dimer arrangement is seen in the clean parts of the surface and the asymmetric configuration can be observed only in the vicinity of the dimer vacancies.[1,5] Then, a recent calculation including an antiferromagnetic arrangement of the spins within the dimer claims that the symmetric configuration for the dimers is more stable one.[6] Detailed observations of the phase transition are expected to give an important information for solving a problem whether the dimers on Si(001) are asymmetric or symmetric.

A recent development in surface physics makes it possible to study two-dimensional critical phenomena such as the order-diorder transition on clean reconstructed surfaces and chemisorbed overlayers by using LEED.[7,8] In the phase transition, the streak pattern plays a significant role and is closely correlated with the short-range ordering in the order-disorder transition. The streak pattern was observed on the Si(001)-2×1 surface[2] and also on the Ge(001)-2×1 surface.[10,11] In the present paper, we have precisely measured the streak patterns correlated with the c(4×2) structure on the clean Si(001) up to temperatures well above the transition. The asymmetric configuration for the dimers is corroborated by the temperature dependence of the streak pattern in LEED. A model derived from the observed results of the streak pattern in LEED is supported by the angle-resolved photoelectron spectroscopy (ARUPS) measurements.

3.2. EXPERIMENTS

The experiments were performed in the system described in previous papers.[2,12] A commercial mirror-polished wafer of Si(001) (p-type, 10 Ω·cm) was washed by acetone or alcohol. The sample was held by a couple of tantalum electrodes in tight contact with the wafer as homogeneously as possible. In the ultrahigh-vacuum chamber, the sample wafer was heated very slowly and kept at 1500 K for 12 hours. After switching off the heating current, the sample was heated up to

1000 K for 10 seconds immediately before the measurements. The clean surface with very low defect density was reproducibly obtained. The amount of the dimer vacancies was estimated to be less than a few percents of the surface atoms by using the STM image.[13]

A video-LEED system equipped with a Varian four-fold LEED optics was used. A video camera using a silicon intensifier target (SIT) tube (Hamamatsu, C1000-12) was applied, since the SIT tube has high sensitivity and good linearity in the intensity measurements. LEED patterns were analyzed by using an image processing system. Each frame was divided into 512×512 sections and each section had a dynamic range of 8 bits. The intensity of the streak pattern is very weak as compared with that of the diffraction spots. Hence, the pattern taking a good signal-to-noise ratio was obtained by accumulating 256 pictures observed independently. However, the intensity in the very weak region showed a step-like change, since each address in the frame memory had only 8 bits.

The temperature dependence of LEED pattern, which was obtained by the accumulation of 256 pictures, is shown in Fig. 1. The incident energy E_p is 36 eV. Figure 2 indicates a relation among scattering spots and streak. This pattern was observed from the double-domain surface. If the observation is made for a single-domain 2×1 surface, which is prepared by a particular surface treatment, the streaks along the [10] direction remain and those along the [01] direction disappear, i.e., the streaks run along the line connecting the vanishing half-order spots of (0 1/2), (1 1/2) etc. in the single-

(a) 450K

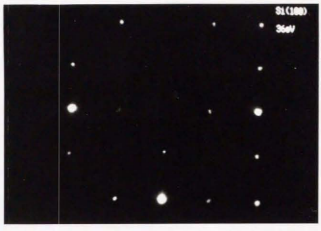

(b) 400K

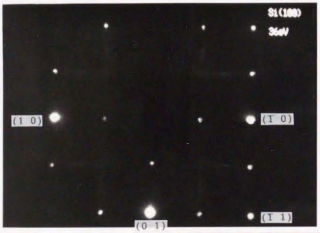

(c) 350K

(d) 320K

(e) 270K

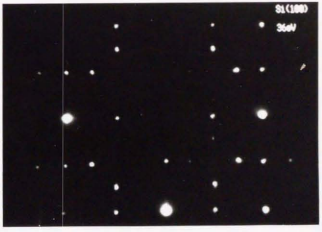

(f) 180K

FIG. 1. Temperature dependence of LEED patterns on Si(001) as a function of specimen temperature. E_p=36 eV.

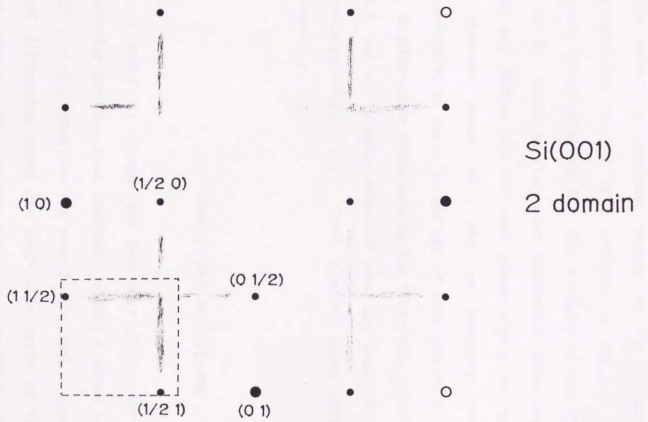

FIG. 2. Schematic of LEED pattern corresponding to FIG. 1(c). An enclosed area is illustrated in FIG. 3 at each temperature.

domain 2×1 surface.

Figure 3 shows the temperature dependence of a bird's-eye view, which show the enclosed region in Fig. 2, at the temperature corresponding to the LEED patterns in Fig. 1. Weak streaks are already observed at 450 K. The intensity of the streaks is enhanced at 400 K. Clear quarter-order diffraction spots appear at 320 K. A weak and diffuse (1/2 1/2) spot characteristic to the p(2×2) structure is observed below 400 K with an intensity independent of the temperature, as shown in the top of each picture of Fig. 3.

Quarter-order spots showing the long-range order appear clearly at 350 K and are steeply enhanced near the transition temperature with decreasing temperature. Then, a clear c(4×2) LEED pattern can be observed at 200 K.

3.3. RESULTS AND DISCUSSIONS

In order to discuss the behaviour of the streak patterns, the scattering profiles were treated. Figure 4 shows the contour of the LEED pattern, which was the same in Fig. 3(c). Upper left and lower right diffraction spots are half-order spots of (1 1/2) and (1/2 1), respectively. The specimen temperature is 350 K, which is well above the transition temperature, 200 K. Clear streaks appear along the <110> directions through half-order spots. The quarter-order spots appear at the middle points of the streaks with decreasing

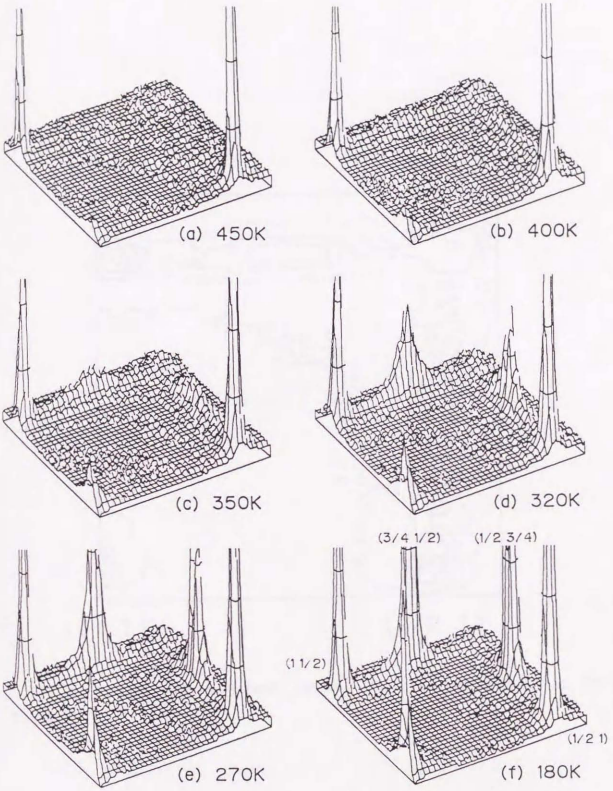

FIG. 3. Bird's-eye view of LEED patterns on Si(001) as a function of specimen temperature. E_p=36 eV.

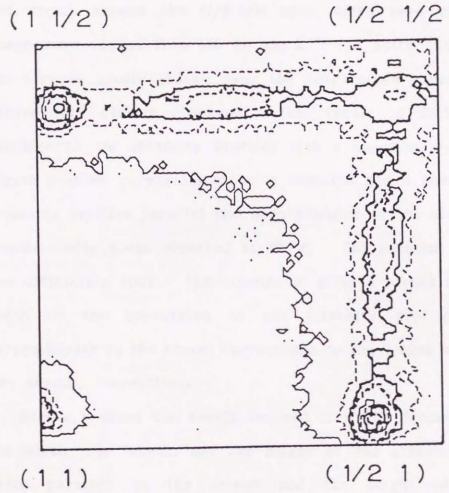

FIG. 4. Contour of a streak pattern in LEED on Si(001) at 350 K. E_p=36 eV.

temperature.

Figure 5(a) shows the intensity profiles parallel to the streak around the (3/4 1/2) spot and Fig. 5(b) shows those perpendicular to the streak around the (1/2 3/4) spot, which were observed in the temperature region from 180 to 450 K. The width and the length of the streaks hardly change over the temperature range, at which the streaks are clearly observed. This result is definitely seen by decomposing the intensity profiles with a Gaussian and a Lorentzian. Figure 6 shows curves fitted by a Gaussian and a Lorentzian for the intensity profiles parallel and perpendicular to the streak around the quarter-order spots observed at 270 K. The Gaussian corresponds to the diffraction spot. The Lorentzian gives a streak pattern and the width of the Lorentzian in the intensity profile parallel and perpendicular to the streak corresponds to the length and the width of the streak, respectively.

Figure 7 shows the result reduced from the decomposed curve for the width, the length, and the height of the streak, and shows the width parallel to the streak and the height of the (3/4 1/2) diffraction spot as a function of temperature. The length and the height of the streak were obtained from the streak around the (3/4 1/2) spot and the width of the streak were obtained from the streak around the (1/2 3/4) spot. The heights of the (1/2 3/4) spot and the streak around the (1/2 3/4) spot are in good agreement with those shown in Fig. 7. The width of the (1/2 3/4) spot perpendicular to the streak shows the same tendency as that of the (3/4 1/2) spot

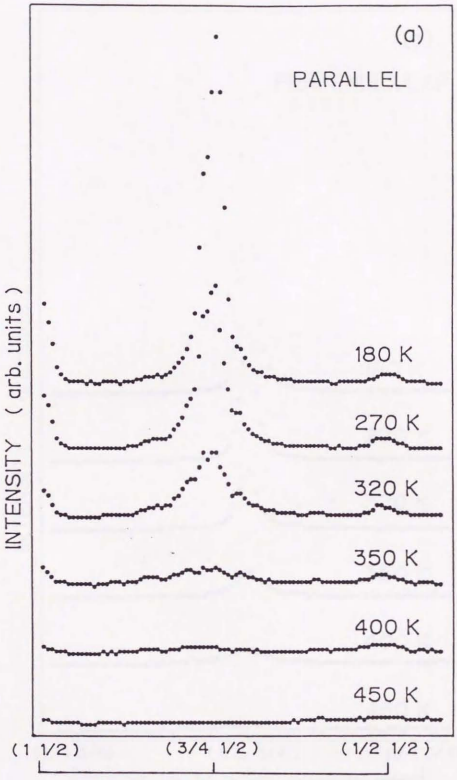

FIG. 5. Temperature dependence of intensity profiles for the streak on the Si(001) surface in the temperature range from 180 to 450 K. (a)Profiles parallel to the streak of the (3/4 1/2) spot and (b)perpendicular to the streak of the (1/2 3/4) spot. E_p=36 eV.

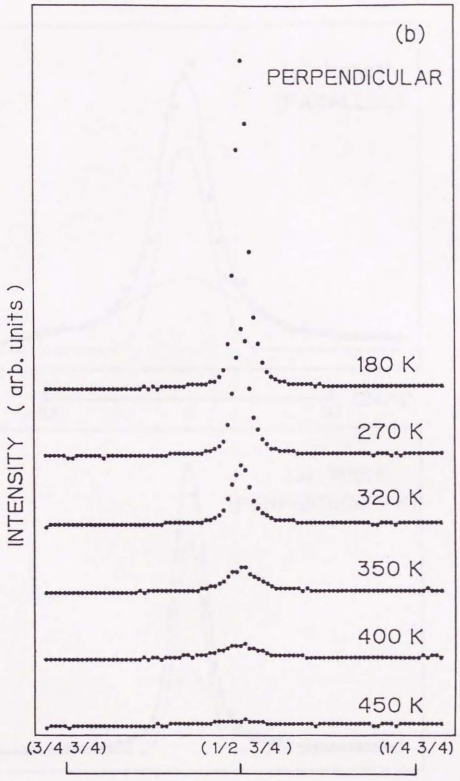

FIG. 5. Temperature dependence of intensity profiles for the streak on the Si(001) surface in the temperature range from 180 to 450 K. (a)Profiles parallel to the streak of the (3/4 1/2) spot and (b)perpendicular to the streak of the (1/2 3/4) spot. E_p=36 eV.

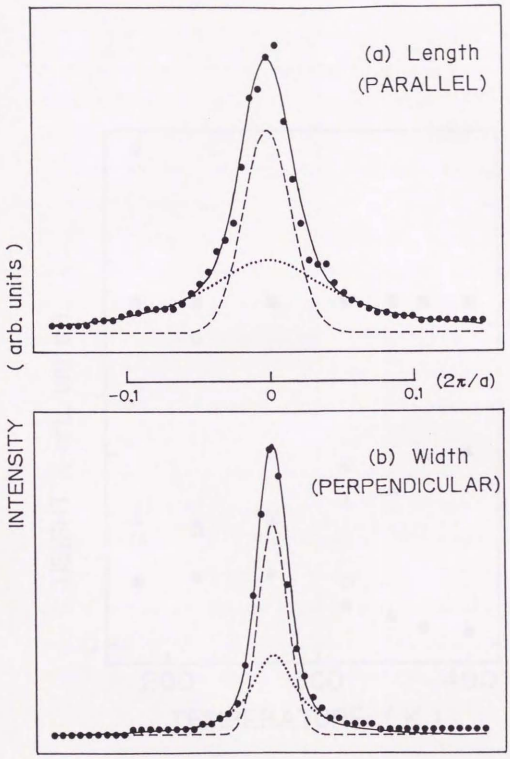

FIG. 6. Deconvolution of the intensity profile observed at 270 K (closed circles) by using a Lorentzian (dotted curve) and a Gaussian (broken curve). Solid line shows the fitting curve, which is the sum of the Lorentzian and the Gaussian.

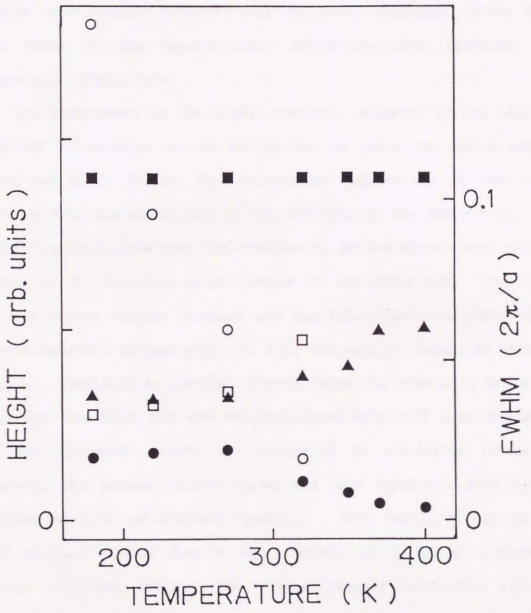

FIG. 7. Temperature dependence of the width (closed triangle), the length (closed square), and the height (closed circle) of the streak, and the width along the streak (open square) and the height (open circle) of the (3/4 1/2) spot, which were obtained by decomposition of the observed intensity profile.

shown in Fig. 7. The length of the streak remains constant, while the width of the streak remains nearly constant and increases gradually above 300 K with increasing temperature. The height of the streak also remains constant and decreases gradually above 300 K. The width of the quarter-order diffraction spot increases with increasing temperature.

The discrepancy in the Si(001) structure observed by the LEED and the STM measurement can be interpreted by using the above results. Then, we shall discuss the temperature dependence of the streak pattern from the standpoint of the ordering in the dimer rows. The streak patterns show that the disordering or the short-range ordering exists in the direction perpendicular to the dimer row. The length of the streak remains constant and the height and the width of the streak scarcely change over the wide temperature range, as shown in Fig. 7. This fact is clearly different from the result of the order-disorder transition for the two-dimensional spin half Ising system.[7,8]

The dynamical effect are concealed in scattering intensities. However, the streak pattern shows the same behaviour with various primary energies of incident electrons. This result is due to that the silicon crystal has a small effect in multiple scattering.[9] Hence, one can analyze the streak pattern with the kinematic diffraction scheme considering only the topmost atomic layer in order to discuss the phase transition. In the kinematic limit, the LEED intensity is the Fourier transform of the two-site correlation function. That is, the scattering intensity I is given by

$$I = \Sigma\Sigma\langle f_i f_j\rangle \exp(i\mathbf{K}\cdot\mathbf{r}_{ij})\exp(-2W), \qquad (1)$$

where f_i is the scattering factor of the ith site (the ith dimer for the present case), $\mathbf{K}$ is the scattering vector, $\mathbf{r}_{ij}$ is the position vector from the ith to the jth site, and exp(-2W) is the Debye-Waller factor.

Here, we define the correlation in fluctuations of density including the scattering factor (scattering density) from the average value at sites i and j as $\langle f_i f_j\rangle = F(\mathbf{r}_{ij}) + \langle f_i\rangle\langle f_j\rangle$, where $\langle f_i\rangle$ is the mean scattering density of the ith site related to the long-range order and $F(\mathbf{r}_{ij})$ is the scattering density-density correlation function describing short-range fluctuations. The Fourier transform of the pair correlation function $F(\mathbf{r}_{ij})$ and $\langle f_i\rangle\langle f_j\rangle$ gives a Lorentzian representing a diffuse pattern and a Gaussian representing a diffraction spot, respectively. Then, the observed profiles can be fitted by the convolution of a Gaussian and a Lorentzian for the system including short-range fluctuations. The Lorentzian gives a streak pattern in the present case. In the two-dimensional system, critical exponents, ν and γ, can be determined from the Lorentzian measured for a succession of temperatures near the transition temperature, T_o. The width of the Lorentzian is given by $|1-T/T_o|^{\nu}$, which changes with temperature.

On the contrary, the experimental result shows that the widths of the Lorentzian parallel and perpendicular to the streak remain

constant in a wide temperature range and only the width perpendicular to the streak increases slightly above 300 K, as seen in Fig. 7. This result is clearly different from that derived from the two-dimensional system[7,8] and cannot be interpretted by a simple theory concerning to the strongly anisotropic two-dimensional Ising system. The integrated intensity versus temperature curve for a quarter-order spot[2] is also impossible to be represented by this system, since Onsager's thermodynamic formula[14] cannot be fitted to the observed curve. On the other hand, the one-dimensional system for the Heisenberg model for infinite spin[15] may be adequate to the interpretation of the streak pattern. Then, we consider that the phase transition on the clean Si(001) surface at 200~400 K is represented by the quasi-one-dimensional system. The spatial Fourier transform of the correlation function of this model is given by the Lorentzian and the width increases gradually with increasing temperature and is nearly constant at 200~400 K. Therefore, the observed result for the streak pattern is considered to be an indication of the one-dimensional system concerning to the arrangement perpendicular to the linear chain, as discussed below.

It is found that the ordering of the asymmetric dimers in the direction parallel to the dimer row remains at 400 K, since the streak pattern appears clearly. However, the coherent length of the ordering along the dimer row decreases gradually above 300 K, since the width of the streak increases gradually. The disordering only between the dimer rows occurs just above 200 K. For the disordering

in the temperature range from 200 to 400 K, the coherent length of diffraction spot decreases across the dimer row of the c(4×2) ordered structure and the component of the local p(2×2) structure increases and broadens with increasing temperature. The order-disorder transition at 200 K appears only in the direction perpendicular to the dimer row and this disordering causes the cooperative change of the ordered buckled dimer rows. That is to say, the A to B transition of a flip-flop type takes place in this disordering, where A and B are the arrangements of the antiferromagnetic ordering in the dimer row, as denoted in Fig. 8(a). This flip-flop type disordering causes the order-disorder transition described by the one-dimensional array consisting of A and B arrangements such as A-B-A-A-A-B-A····. The Si(001) surface is illustrated by the quasi-one-dimensional system at high temperature.

Although the conversion time between A and B arrangements is longer than the period of the lattice vibration, $\sim 10^{-9}$ s, at the surface, the conversion time is considered to be much shorter than the scanning time on an atom in the STM observation. Since the flip-flop motion occurs frequently, the time-averaged STM image is observed and shows the apparent symmetric dimer feature.

The strongly anisotropic two-dimensional phase transition is clearly different from the result obtained by a Monte Carlo simulation by Saxena et al.,[4] since the simulation shows the isotropically randomized spin system. In this simulation the coupling constants derived from the tight-binding approximation were used, i.e. H/V=-0.38

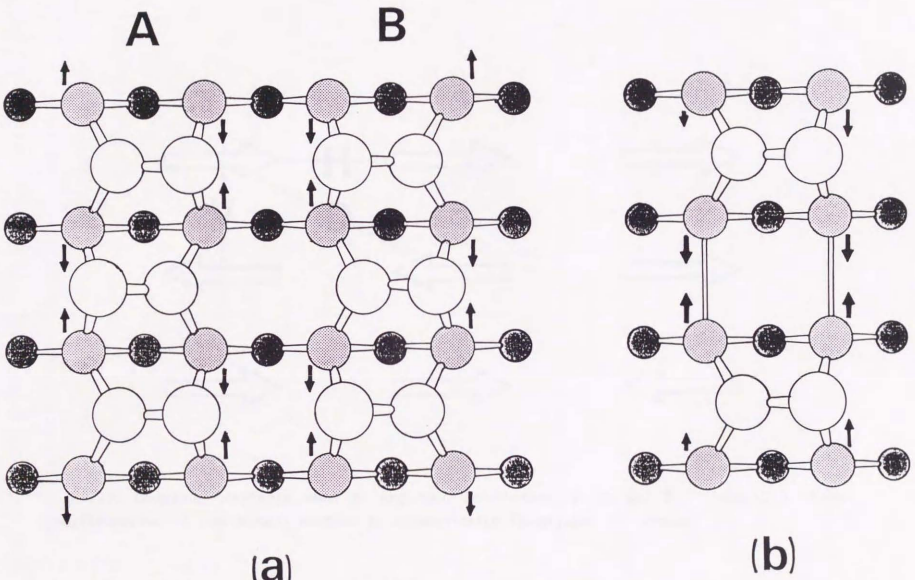

FIG. 8. Top view of the SI(001) surface of (a) the clean c(4×2) surface and (b) the surface with a dimer vacancy. The arrows show the displacement vector of the second-layer atoms for the stabilized arrangement of the buckling configuration.

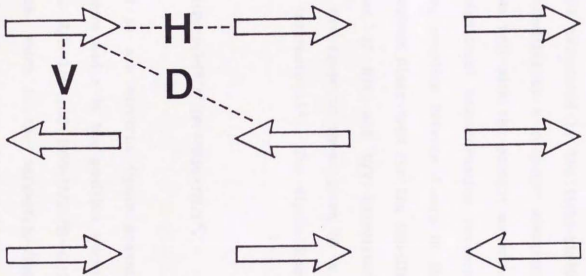

FIG. 9. Coupling constants used in the spin Hamiltonian, V, H, and D. Asymmetric dimer configuration of the Si(001) surface is schematically illustrated by arrows.

and D/V=-0.15, where the coupling constants for the spin Hamiltonian, V, H, and D, are shown in Fig. 9. The experimental result of the highly anisotropic behavior shows that the ratio H/V is much smaller than the value calculated by the tight-binding approximation. This situation is clarified by a computer simulation and the result using H/V~0.05 agrees well with the present experimental result.[16,17] The cooperative structural transformation between A and B arrangements shows a strong coupling between dimers in the dimer row and a weak interaction between dimer rows for the two-dimensional system.

The values of H/V and D/V calculated by the tight-binding approximation are close to those given by a classical scheme of the dipole-dipole interaction.[18] The dipole-dipole interaction potential is given by

$$U = [(\mathbf{p}_1 \cdot \mathbf{p}_2)-(3/\mathbf{r}^2)(\mathbf{p}_1 \cdot \mathbf{r})(\mathbf{p}_2 \cdot \mathbf{r})]/\mathbf{r}^3, \qquad (2)$$

where $\mathbf{p}_1$ and $\mathbf{p}_2$ are electric dipole moments corresponding to the asymmetric dimers and $\mathbf{r}$ is the position vector from $\mathbf{p}_1$ to $\mathbf{p}_2$. From this equation, H/V=-1/4 and D/V=-(7/25$\sqrt{5}$)=-0.125 are obtained in the present system, which is the asymmetric-dimer arrangements on the Si(001) surface, and are very close to those calculated by the tight-binding approximation.

Since the experimental results are reproduced by the much smaller value of H/V than that calculated from the dipole-dipole interaction, the antiferromagnetic ordering is highly stabilized in the dimer row

as compared with the ferromagnetic ordering. This strong coupling between nearest-neighbor dimers along the dimer row is considered to be caused by the feasible displacement of the second-layer atoms in addition to the dipole-dipole interaction. The buckling arrangement in the antiferromagnetic ordering is stabilized by the displacement of the second-layer atoms along the dimer row in the opposite direction between the nearest-neighbor atoms, as shown by arrows in Fig. 8(a), where the Si-Si backbond distance remains constant. On the contrary, the displacement of the second layer atoms without change of the Si-Si backbond length is hard in the ferromagnetic ordering. A similar argument has been discussed in the Ge(001) surface.[19]

In order to verify the argument that the antiferromagnetic ordering in the dimer row remains up to 400 K, we measured the temperature dependence of ARUPS up to temperatures well above the transition by using photon energy of 16.8 eV (Ne I). The specimen temperature was changed from 150 to 1190 K. The spectra at high temperatures were measured by alternating between aquisition of photoelectrons and sample heating by a direct current every 20 ms. This method kept the sample temperature stable and gave an electric-field-free condition during the ARUPS measurements. The temperature was monitored by an optical pyrometer and a radiation thermometer. The initial-state energy dispersion for the surface state did not change above and below the transition temperature of the surface structure. The measured dispersions are nearly the same as those observed in an earlier study by Uhrberg et al.[20] Enta et al. also

concluded that this surface occured order-disorder transition from the result of the dispersion relation between above and below the transition temperature.[21]

Figure 10 shows the temperature dependence of the UPS spectra from the surface state in the normal emission, i.e. at the Γ point. The energy at Γ is most sensitive to the problem whether the surface dimer configuration is symmetric or asymmetric.[23] The peak position does not shift with temperature. The peak height decreases linearly and the peak width (full width at half maximum) increases with increasing temperature, as shown in Fig. 11. The integral photoemission intensity from the surface state obtained by product of the height and the width is nearly constant against temperature. These results show that the local interaction in the surface state shows no abrupt change above the transition temperature. The broadening of the surface state peak is considered to occur due to the thermal agitation in the antiferromagnetic ordering of the dimer row. This interpretation is consistent with the result obtained from the temperature dependence of the streak patterns in LEED.

Finally, we shall discuss the reason why the asymmetric dimer arrangement is seen in the vicinity of the dimer vacancies in STM images.[1] On the Si(001) surface, missing-dimer defects can reduce the number of dangling bonds and lower the electronic energy. However, the elastic strain energy increases due to the distorsion field indicated by the arrows in Fig. 8(b). This distorsion field occasionally makes the periodically arranged defect side by side in

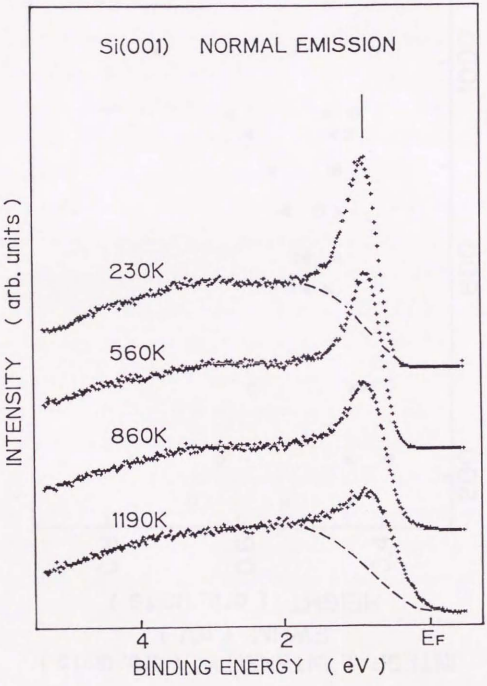

FIG. 10. ARUPS spectra from the surface state on Si(001) in normal emission as a function of specimen temperature. $h\nu$=16.8 eV (Ne I). Dashed line indicates a photoemission from the bulk,[22] which is used to extract the surface compornent.

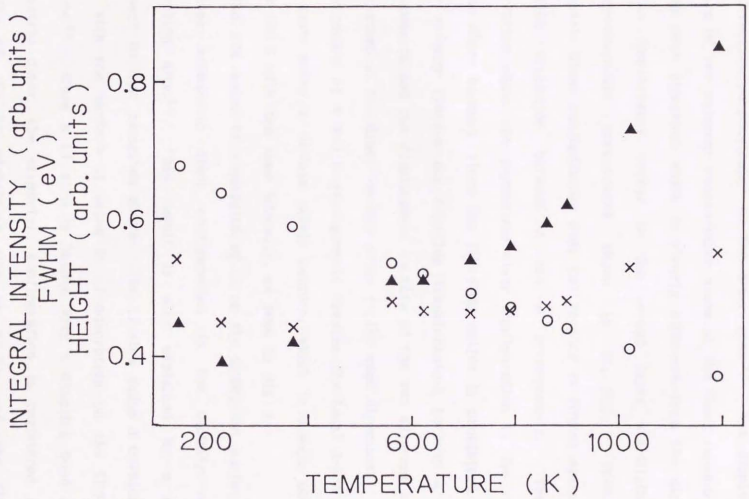

FIG. 11. Temperature dependence of integral intensity (cross), the peak height(open circle), and the peak width (closed triangle), full width at half maximum, in ARUPS spectra at the Γ point from the surface state on Si(001). $h\nu$=16.8 eV (Ne I).

the direction perpendicular to the dimer rows.[24] The displacement vectors of two adjacent second-layer atoms at the dimer vacancy point in the same direction, which is clearly different from the direction of the displacement vector in the second layer stabilizing the antiferromagnetic arrangement shown in Fig. 8(a). Then, the asymmetric dimer configuration near the vacancy is frozen against the flip-flop transition between A and B arrangements. The STM observation shows the asymmetric dimer configuration in the vicinity of the dimer vacancy, since the flip-flop motion is prohibited. The dimer vacancy freezes the flip-flop transformation between A and B arrangements and the displacement vectors of the two adjacent second-layer atoms at the dimer vacancy point in the same direction. Hence, the sequence of A and B arrangements creates the local A-A-A array. This part makes a diffuse p(2×2) pattern, which is always observed below 400 K with the same intensity, as seen in Fig. 3.

The STM images of adsorption of Li on the Si(001)-2×1 surface show a clear asymmetric dimer configuration in the vicinity of the adsorption site.[25] This result is also explained by a similar argument to that described above. The Li atom makes a covalent-like bond with the surface Si atoms in Li adsorption on the Si(001)-2×1 surface.[26] Since a Li atom is bonded with a dangling bond of the asymmetric dimer, the asymmetric configuration is registered in the vicinity of the Li adsorption site on Si(001) and the flip-flop transformation between A and B arrangements is forbidden.

REFERENCES

[1]R. M. Tromp, R. J. Hamers, and J. E. Demuth, Phys. Rev. Lett. 55, 1303 (1985).

[2]T. Tabata, T. Aruga, and Y. Murata, Surf. Sci. 179, L63 (1987).

[3]J. Ihm, D. H. Lee, J. D. Joannopoulos, and J. J. Xiong, Phys. Rev. Lett. 51, 1872 (1982).

[4]A. Saxena, E. T. Gawlinski, and J. D. Gunton, Surf. Sci. 160, 618 (1985).

[5]R. J. Hamers, Ph. Avouris, and F. Bozso, Phys. Rev. Lett. 59, 2071 (1987).

[6]E. Artacho and F. Yandurain, Phys. Rev. Lett. 62, 2491 (1989).

[7]R. F. Willis, in *Dynamical Phenomena at Surfaces, Interfaces and Superlattices*, ed. by F. Nizzoli, K.-H. Rieder, and R. F. Willis (Springer, Berlin, 1985) p.126.

[8]T. L. Einstein, in *Chemistry and Physics of Solid Surfaces* VII, ed. by R. Vanselow and R. Howe (Springer, Berlin, 1988) p.307.

[9]M. A. Van Hove, W. H. Weinberg, and C. -M. Chan, *Low-Energy Electron Diffraction*, (Springer-Verlag, Berlin, 1986).

[10]S. D. Kevan, Phys. Rev. B 32, 2344 (1985).

[11]R. J. Culbertson, Y. Kuk, and L. C. Feldman, Surf. Sci. 167, 127 (1986).

[12]Y. Murata, H. Tochihara, and M. Kubota, in *Metallization and Metal-Semiconductor Interfaces*, ed. by I. P. Batra (Plenum, New York, 1989) p.367

[13]T. Hashizume, Y. Hasegawa, I. Kamiya, T. Ide, I. Sumita, S. Hyodo, T. Sakurai, H. Tochihara, M. Kubota, and Y. Murata, J. Vac. Sci. Technol. A 8, 233 (1990).

[14]L. Onsager, Phys. Rev. 65, 117 (1944); C. N. Yang, Phys. Rev. 85, 808 (1952); C. H. Chang, Phys. Rev. 88, 1422 (1952); E. W. Montroll, R. B. Potts, and J. C. Ward, J. Math. Phys. 4, 308 (1963).

[15]M. E. Fisher, Am. J. Phys. 32, 343 (1964).

[16]K. Kakitani and A. Yoshimori, in *Ordering at Surfaces and Interfaces*, ed. by A. Yoshimori and T. Shinjo (Springer-Verlag, Berlin, 1991) in press.

[17]M. Kubota, N. V. Richardson, and Y. Murata, to be published.

[18]Y. Murata, M. Kubota, and T. Tabata, in *Ordering at Surfaces and Interfaces*, ed. by A. Yoshimori and T. Shinjo (Springer-Verlag, Berlin, 1991) in press.

[19]M. C. Payne, M. Needels, and J. D. Joannopoulos, J. Phys.: Condens. Matter 1, SB63 (1989).

[20]R. I. Uhrberg, G. V. Hansson, J. M. Nicholls, and S. A. Flodstrom, Phys. Rev. B 24, 4684 (1981).

[21]Y. Enta, S. Suzuki, and S. Kono, Phys. Rev. Lett. 65, 2704 (1990)

[22]F. J. Himpsel and Th. Fauster, J. Vac. Sci. Technol. A 2, 815 (1984).

[23]D. J. Chadi, Phys. Rev. Lett. 43, 43 (1979).

[24]T. Aruga and Y. Murata, Phys. Rev. B 34, 5654 (1986).

[25]Y. Hasegawa, I. Kamiya, T. Hashizume, T. Sakurai, H. Tochihara, M. Kubota, and Y. Murata, Phys. Rev. B 41, 9688 (1990).

[26]H. Tochihara and Y. Murata, Surf. Sci. 215, L323 (1989).

Chapter 4

Silicide formation in the Au-Si interface

4.1. INTRODUCTION

Transition metals are known to react with Si immediately after deposition on the clean Si surface and silicides are produced. The Schottky barrier height is significantly affected by silicide formation in the interface between the metal overlayer and the Si substrate.[1] Then, the phenomenon of room-temperature-alloyed interface formation (RTAIF) at metal-semiconductor contact is one of the most important problems both in the field of pure science and in the field of electronic devices, among many problems in metal-semiconductor contact systems.[2-5] Especially, the Au(film)-Si(substrate) contact is an interesting system, in which intermixing of Au with Si at the interface and oxidation of Si on the specimen surface take place. These results were first obtained by using theRutherford backscattering spectrometry (RBS)[6] and Au-Si alloy formation was confirmed by more microscopic Auger electron spectroscopy (AES)[7] followed by many works.[8-11] On the other hand, the Ag(film)-Si(substrate) system is considered to be non-reacting, i.e., the Ag-Si contact shows no alloy formation[12-14] The common sense in chemistry implies that Au has much lower reactivity with Si than Ag. However, the above result is clearly contradictory. The present study carried out in order to elucidate the mechanism of Au-Si alloy formation.

Several models have been proposed for the origin of RTAIF: (I) the "screening model",[15,16] in which it is proposed that an

intermixing reaction is induced through a screening effect of metallic electrons in an overlayer metal film formed by the deposition of metal atoms; (II) the "interstitial model",[17-19] in which it is claimed that a silicide-like compound is formed, or that an intermixing occurs between metal and semiconductor atoms, immediately at the beginning stage of the metal-atom deposition at coverages much less than one monolayer, $\Theta(M)<<1$, where $\Theta(M)=1$ means one monolayer (ML) coverage of metal atoms on a crystal substrate and is defined by $\sim 7.8\times10^{14}$ atoms$\cdot$cm^{-2} on a Si(111) surface; and (III) the "thermodynamical model", which classifies metal-semiconductor contact systems into reacting and non-reacting systems by using the quantity defined as the heat of reaction, ΔH_R.[3]

The Au-Si(111)7×7 system was studied by Braicovich et al.[18] by using photoemission. In the present study, the initial stage of metal deposition in the coverage range below 2~3 ML was carefully studied by using photoemission through the chemical shift of the core levels and the splitting of the valence band, and finally, by using the resonant photoemission due to the valence band mixing in the Au-Si system, in order to examine covalent-like-bond formation. From these experimental data, the change of the bonding structure between Au and Si atoms on the surface is discussed. On the contrary to these results, no enhancement was observed for Ag($\Theta\sim1$)/Si(111)-(2×1) in the resonant-photoemission condition and no chemical bond is formed between Ag and Si. On the basis of these experimental observations,

it will be shown that a covalent-like chemical-bond formation at $\Theta(M) \leq 1$ is important for RTAIF in M/Si(111) systems at $\Theta(M) \geq 1$. A new model, the "chemical bonding model", is proposed to explain the initial stage of metallic alloy or compound formation in the metal-silicon system.

4.2. EXPERIMENTS

The present study was carried out in the BL-2 system of the SOR Ring in the Synchrotron Radiation Laboratory of the Institute for Solid State Physics at the University of Tokyo. Analyzing and sample-preparation chambers were constructed by a stainless-steel ultrahigh-vacuum (UHV) system consisting of conventional ion and titanium sublimation pumps; $\sim 3 \times 10^{-9}$ Pa in the analyzing chamber when the photon source was switched on and low-10^{-8} Pa range in the sample-preparation chamber. The Si(111)-(2×1) clean surface was prepared by cleaving a block of a silicon single crystal in the sample-preparation chamber. The effect of the surface-step density has not been examined. It is difficult to observe the surface-step density on the cleaved face, though the surface-step density can be estimated from the transition temperature of irreversible transition from (2×1) to (7×7) on the Si(111) cleaved face. Au- and Ag-atom deposition was performed by using W baskets. Thickness of Au and Ag layers was estimated by using a quartz thickness monitor. LEED patterns were observed as a function of the Au or Ag coverage. A spectrometer used

for electron energy analysis was a double-pass cylindrical-mirror analyzer(CMA) with a retarding grid at the entrance. Photoemission spectra were taken under angle-integrated conditions, where the incident photon beam was 47.7° to the specimen surface and 90° to the CMA axis. The photon energy ($h\nu$) was varied between 30 and 160 eV according to experimental requirements. The total energy resolution was 0.7 eV or better. The Fermi level (E_F) position was determined by using the metallic edge of the Au signal from a gold film connected electrically to the specimen.

4.3. RESULTS and DISCUSSIONS

4.3.1. Coverage dependence of the core level shift

A typical photoemission spectrum from core levels, Si(2*p*) and Au(4*f*), is shown in Fig. 1 for Au(~10 ML) on the Si(111)2×1 surface at $h\nu$=115 eV. The binding energies of Si(2*p*) and Au(4*f*) as a function of coverage are shown in Fig. 2, where the binding energy of Au($4f_{7/2}$) was used for Au(4*f*). The binding energy of the core level was deduced from the Fermi edge of the Au film measured at the same photon energy. The coverage is expressed in monolayer units. With increasing Au coverage the binding energy of Au(4*f*) increases slightly at the beginning of the Au deposition and decreases later to saturate at a value between the binding energy of pure gold and that at the

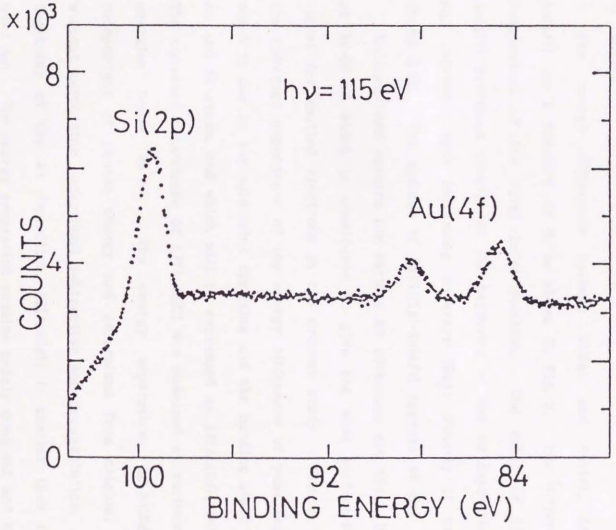

FIG. 1. Core level photoemission spectrum from Si(2*p*) and Au(4*f*) of a specimen Au(~10 ML)-SI(111)2×1 at $h\nu$=115 eV.

lowest coverage, where the signal of Au($4f$) was first observed. The binding-energy change of Si($2p$) is in the opposite direction to that of Au($4f$).

The energy difference between Si($2p$) and Au($4f$), ΔE[Si($2p$)-Au($4f$)], as a function of Θ, is shown in Fig. 3. The difference is independent of the Fermi level position. The value of ΔE[Si($2p$)-Au($4f$)] decreases clearly at the beginning of the Au deposition ($\Theta \lesssim 1$) and increases with increasing coverage ($\Theta \gtrsim 1$). Finally it saturates above Θ=20. The minimum of ΔE[Si($2p$)-Au($4f$)] appears at $\Theta \simeq 1$.

Valence band spectra for various Au coverages are shown in Fig. 4 at $h\nu$=90 eV which is considered to give the most surface-sensitive signal for emitted electrons in the present study. Figure. 5 shows the coverage dependence of the energy difference of peak separation which is due to the spin-orbit spritting and the bonding state between Au and Si atoms, and which will be expressed as ΔE[Au($5d$)] for short. The coverage dependence of ΔE[Au($5d$)] was measured at various photon energies below 90 eV. The energy separation, ΔE[Au($5d$)], was independent of photon energy and determined from original spectra without performing background subtraction and deconvolution. At the beginning of the Au deposition, ΔE[Au($5d$)] is smaller than that for pure Au. The energy separation remains nearly constant and increases above $\Theta \simeq 1$. Furthermore, even at the highest coverage ($\Theta \simeq 100$) the spectral shape is quite different from that of pure gold, as seen in Fig. 4. This difference immediately indicates that the surface of the specimen obtained after the Au deposition ($\Theta \simeq 100$) on Si(111)2×1 is

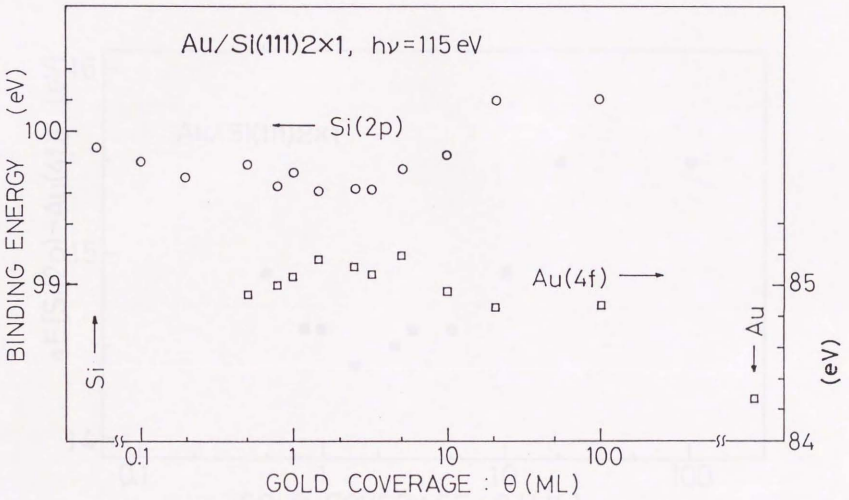

FIG. 2. Au coverage (θ in ML) dependence of Si(2*p*) and Au(4*f*) binding energies. The binding energy is deduced by using E_F positions determined from valence band spectra of Au. Arrows of Si and Au indicate the values of clean silicon and gold surfaces, respectively.

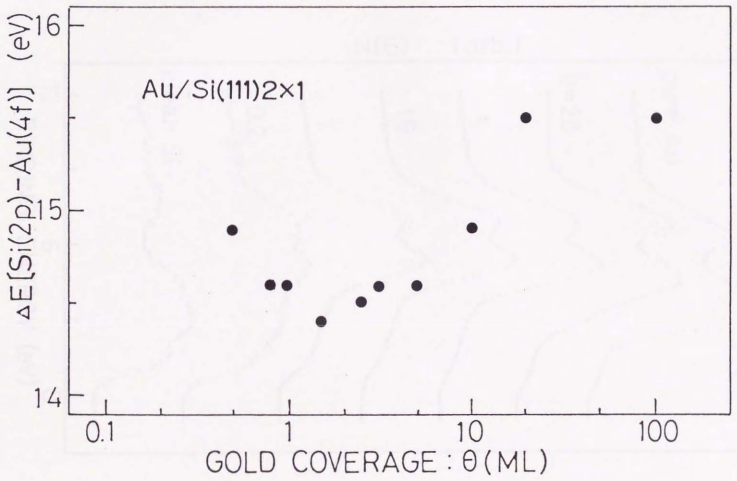

FIG. 3. Energy difference between Si(2*p*) and Au(4*f*) lines. $\Delta E[Si(2p)\text{-}Au(4f)]$, as a function of coverage θ (ML).

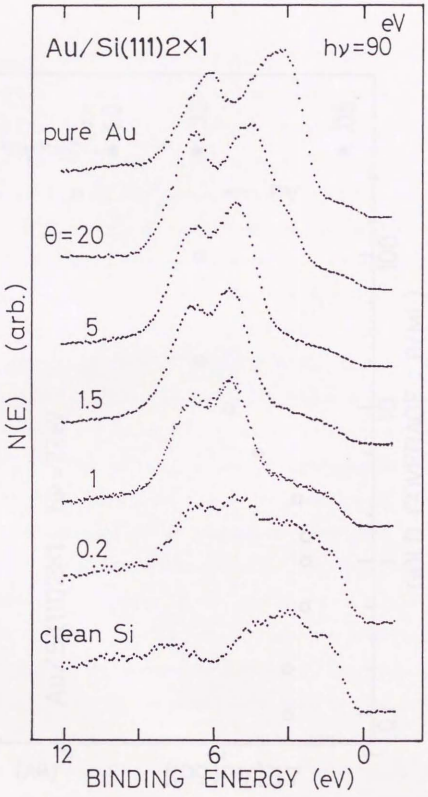

FIG. 4. Valence band photoemission spectra as a function of the Au coverage. hν=90 eV.

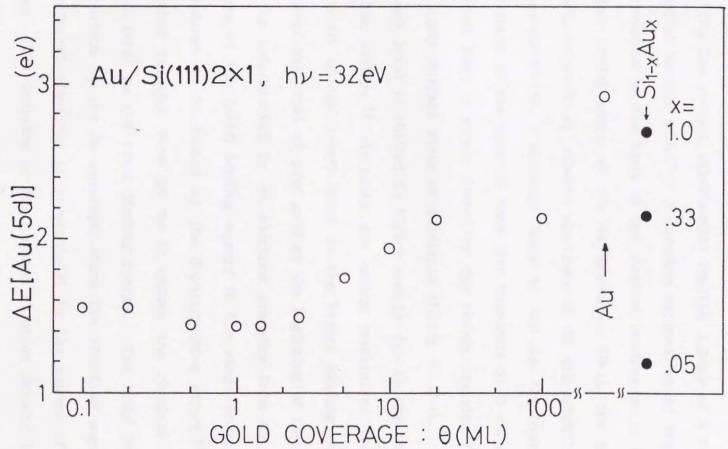

FIG. 5. Au coverage dependence of $\Delta E[Au(5d)]$, the energy difference between $Au(5d_{5/2})$ and $Au(5d_{3/2})$. XPS results on alloys of Au_xSi_{1-x} [20] are also shown by filled circle, where x values are shown in the figure. The arrow indicates the value of the clean gold surface.

different from the clean Au surface.

From the present experimental results, I propose a new model: the "chemical bonding model". A possible explanation of the experimental observations on the basis of the chemical bonding model is as follows. In the initial stage of the Au deposition ($\theta<1$), the Au-Si bond is formed, in which $6s$ valence electrons of Au are slightly transferred to substrate Si. Although both $6s$ and $5d$ electrons of Au may contribute to the chemical bond with substrate Si, I consider that the chemical bond is mainly formed by the charge transfer from Au($6s$) to the empty surface state of substrate silicon at $\theta<<1$. Since the Au valence level is shifted to higher energy due to the image potential on the surface,[21] electrons are easily transferred from Au to Si. The shift of the Au($4f$) level to the higher binding energy side as compared with that of pure gold at the beginning of the Au deposition can be interpretted by an electron transfer from Au to Si. The change of the Au($4f$) binding energy in the range from $\theta=0.5$ to 1 is considered to be caused by the depolarization effect.[22] Also, the electron transfer from Au to Si causes the chemical shift of the Si($2p$) level to the lower binding energy. The Si($2p$) level shifts in proportion to the Au coverage, since the effective magnitude of the transferred electrons is proportional to the number of adsorbed Au atoms. The decrease of the valence electron density in an Au atom causes the decrease of the energy difference of the separation in the Au(5d) level as compared with that of pure gold. These considerations are in good agreement with the experimental results in

the range of $\Theta<1$, as seen in Figs. 2 and 5.

The charge transfer is considered to form the non-metallic bond between Au and Si atoms. After the non-metallic bond formation between an Au atom and a Si dangling bond, backbonds of the surface Si atom are weakened. After further deposition beyond Au monolayer coverage, Au atoms are located in the hollow site near the surface silicon network and easily form the Au-Si bond by breaking off the weakened backbond rather than the Au metal cluster on the surface. The binding energies of Si($2p$) and Au($4f$) change at $\Theta\geq1$ in the opposite direction from those of $\Theta\leq1$, i.e. to the higher binding energy in Si($2p$) and to the lower binding energy in Au($4f$). The obvious change in the binding energies at $\Theta\simeq1$ indicates that the nature of the chemical bond of Au-Si changes there. The Au-Si bond becomes covalent-bond-like at $\Theta\simeq1$, since the depolarization shift of the Au valence level reduces the magnitude of the transferred electrons, while the main contribution in the chemical bond below 1 ML is the charge transfer from Au($6s$) into the unoccupied level of the Si dangling bond state, i.e. ionic-bond-like. At the beginning of Au deposition, the Au($6s$) level is shifted upward in energy due to the image potential, as the Au atom approaches the Si surface. Hence, the Au($6s$) electrons are transferred into the unoccupied surface state of Si.

Similar changes can be seen in the spectra of Au($5d$). The separation of ΔE[Au($5d$)] shows a slight decrease until $\Theta\simeq1$ and a considerable increase above $\Theta\simeq1$, as can be seen in Fig. 5. The

change in the binding energies of Si($2p$) and Au($4f$) at $\Theta \simeq 1$ can be seen more clearly in Fig. 3, where the difference of the binding energies between Si($2p$) and Au($4f$) is shown. In the value of ΔE[Si($2p$)-Au($4f$)], there is no ambiguity due to the determination of the Fermi level (E_F) at each coverage. The data in Fig. 3 again claim that the surface electronic structure is different between below and above $\Theta \simeq 1$.

Above $\Theta \simeq 20$, the binding energies of Si($2p$) and Au($4f$) and the splitting of Au($5d$) show no change at all. These saturated values of Au at $\Theta \geq 20$ are different from those of the clean Au surface. In this range ($20 \leq \Theta \leq 100$), small amounts of silicon atoms exist in the very surface region of the gold film formed on the Si surface, where Si atoms make the metallic bond with surrounding gold atoms, as was clarified before,[7,15] i.e. Au-Si metallic alloy has been found on the surface.

I observed the Ag-coverage dependence of the valence-band spectrum of Ag/Si(111)-(2×1) deposited at room temperature. An important feature of the results is the fact that the saturation values of both the full width at half maximum (FWHM) of the Ag($4d$) signal, E_v[Ag($4d$)], and ΔE[Ag($4d$)], the energy difference ΔE[Ag($4d_{5/2}$)-Ag($4d_{3/2}$)], are exactly the same as those of pure Ag, as seen in Fig. 6. Figure 7 shows that the binding energy of Si($2p$) is nearly constant over a wide Ag-coverage region. An experimental result of the LEED study on Au and Ag/Si(111)-(2×1) is shown in Table 1. The results tell us that Ag atoms disperse almost uniformly on the Si(111) surface without making islands until Θ(Ag)~0.7. Ag atoms form a two-

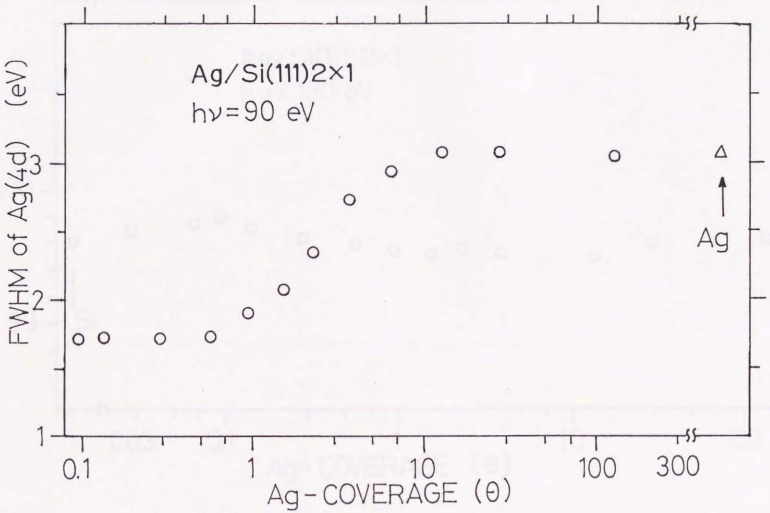

FIG. 6. Ag coverage dependence of $\Delta E[Ag(4d)]$, the energy difference between $Ag(4d_{5/2})$ and $Ag(4d_{3/2})$. The arrow indicates the value of the clean silver surface.

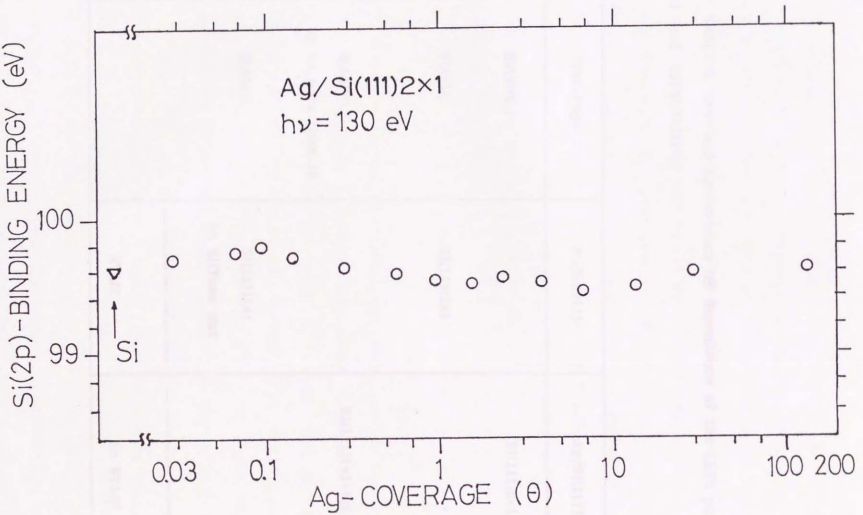

FIG. 7. Ag coverage (θ in ML) dependence of Si(2*p*) binding energies.

TABLE 1. Au- and Ag-coverage (Θ) dependence of the LEED pattern on Au and Ag/Si(111)2×1.

Coverage	Au/Si(111)	Ag/Si(111)
Θ(Ag)<0.7		Si(111)2×1
Θ(Au)<1	Si(111)2×1	
Θ(Ag)>0.7 up to more than 10		Si(111)1×1+Ag(111)1×1
Θ(Au)>1	Si(111)1×1 to diffuse out	
	RTAIF	No RTAIF

dimensional layer up to Θ(Ag)~0.7 and grow as islands above Θ(Ag)~0.7, i.e., Ag atoms deposited on the Si(111)-(2×1) surface grow in the Stranski-Krastanov mode, as is the case in Ag/Si(111)-(7×7).[12]

From these comparisons, we can tentatively deduce the following conclusions: A room-temperature deposition of Ag on Si(111)-(2×1) does not induce RTAIF, while the Au deposition on Si(111)-(2×1) does. Namely, Ag islands grow on the surface without including any alloying due to the deposition of Ag atoms on the Si(111)-(2×1) surface, which is consistent with the previous report on Ag/Si(111)-(7×7).[12]

4.3.2. Resonant photoemission

I have succeeded in observing an enhancement in the valence-band photoemission spectrum mainly contributed from Au(5*d*) electrons of Au(Θ~1)/Si(111)-(2×1) at the incident photon energies of ~100 eV, where the threshold energy of the Si(2*p*) core excitation is 99.5 eV. The experimental data given in Fig. 8 clearly show the following facts. (a) No special change appears in valence-band spectra at $h\upsilon$<99 eV. (b) At incident photon energies above the threshold, $h\upsilon$=99.5 eV, the photoemission spectra from the valence band at E_b~7 eV show an enhancement in their intensity. Such an enhancement cannot be seen in the Au(5*d*) signal of pure Au.[23] It should be noted, in this photon energy region, that another structure indicated by an arrow *A* appears, which is due to Si(*LVV*) Auger electron excitation.

Considering the fact that there is an enhancement of the valence-band spectrum of pure Si including that due to the Auger electron excitation,[24] background signals in the spectra are carefully subtracted. In the background subtraction, the existence of Au atoms by an amount of Θ(Au)~1 is, of course, taken into account. Normalized intensity of the valence-band signal at E_b~7 eV, I(7 eV), is shown in Fig. 9 as a function of the incident photon energy. The normalization is performed by using the intensity of the valence-band photoemission from E_b~5 eV at $h\nu$=100 eV. One can clearly see a Fano-type resonance in Fig. 9.[25] The preferential enhancement of I(7 eV) is consistent with the experimental result that the photoemission peak at E_b~7 eV has a slight dispersion in Au/Si(111).[26] The peak at E_b~7 eV must correspond to the bonding state of Au(5d) with Si(3s,3p). This resonance-like enhancement clearly shows the intermixing of valence electrons between Au and Si atoms in Au/Si(111)-(2×1) at Θ(Au)~1, i.e., Au and Si atoms make a covalent-like bond. A similar resonance-like enhancement has been reported for the Al-GaAs system.[27]

The situation is quite different in Ag/Si(111)-(2×1). Photoemission spectra of Ag(Θ~1)/Si(111)-(2×1) corresponding to those of Fig. 8 are shown in Fig. 10. From this experimental result, it can be deduced that there is no special enhancement of the Ag(4d) signal. Though a slight enhancement of I(6 eV) relative to I(5.5 eV) is seen at photon energies above 99.5 eV in Fig. 10, a similar enhancement can be observed in pure Ag, as shown in Fig. 11. Therefore, this enhancement is explained by the band (formation)

effect in Ag. In other words, the bulk-like Ag islands are formed at Θ(Ag)~1. This observation is consistent with the above result that the island formation starts at Θ(Ag)~0.7. Hence, it can be concluded that no strong chemical bond is formed between Ag and Si atoms at the stage of Θ(Ag)~1.

It can be said from the results shown in Figs. 8, 9, and 10 that the formation of a covalent-like bond between *M* and Si atoms at the beginning stage of the *M*-atom deposition takes an important role in inducing RTAIF. In Au/Si(111)-(2×1), the covalent-like bond is formed between Au and Si atoms at Θ(Au)~1, which is confirmed by the observation of the existence of a resonance-like enhancement of the Au(5*d*)-related photoemission signal at $h\nu$~100 eV. A metallic Au-Si alloy formed above Θ(Au)~1 on the Si(111) surface changes its composition during the course of the Au deposition between Θ(Au)~1 and Θ(Au)~10 in such a way that the concentration of Au becomes rich. On the other hand, in Ag/Si(111)-(2×1) there is no strong chemical bond, as is clarified by several experimental observations. This is the reason why the Ag-atom deposition does not induce a Ag-Si alloy formation, i.e., RTAIF, on the Si(111)-(2×1) surface. Indeed, pure Ag islands grow epitaxially on the Si(111) surface.

From the discussion given above, it can be concluded that the covalent-like chemical-bond formation at the initial stage of metal-atom deposition, $\Theta(M) \leq 1$, plays an important role in the course of the alloyed interface formation in metal-semiconductor contact systems at room temperature. It is concluded that the covalent-like-bond

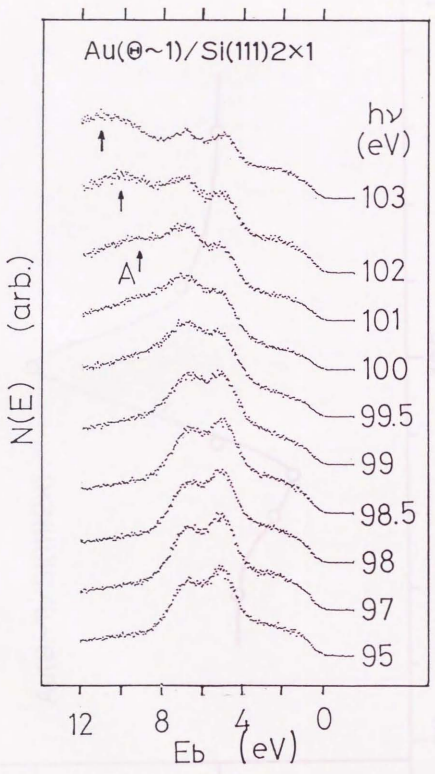

FIG. 8. Valence-band photoemission spectra of Au(Θ~1)/Si(111)-(2×1) at photon energies around the threshold of the Si(2*p*) core excitation: $h\nu$=99.5 eV.

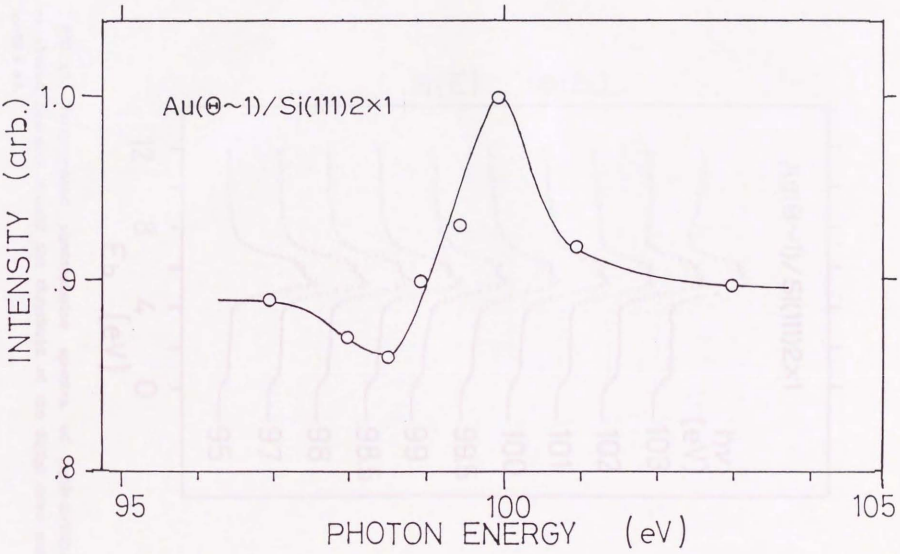

FIG. 9. Plot of the photoemission intensity at E_b=7 eV from FIG. 8 against the incident photon energy. The effect of Si(*LVV*) Auger electron emission has been subtracted. The intensity is normalized by the photoemission intensity at E_b=5 eV of

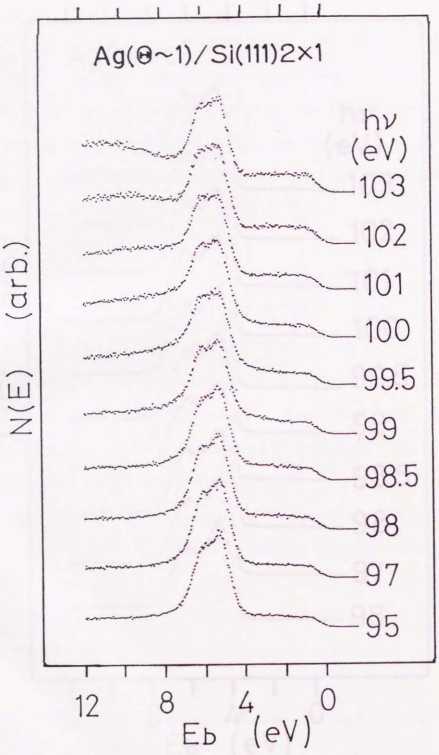

FIG. 10. Valence-band photoemission spectra of Ag(Θ~1)/Si(111)-(2×1) at photon energies around the threshold of the Si(2*p*) core excitation: $h\nu$=99.5 eV.

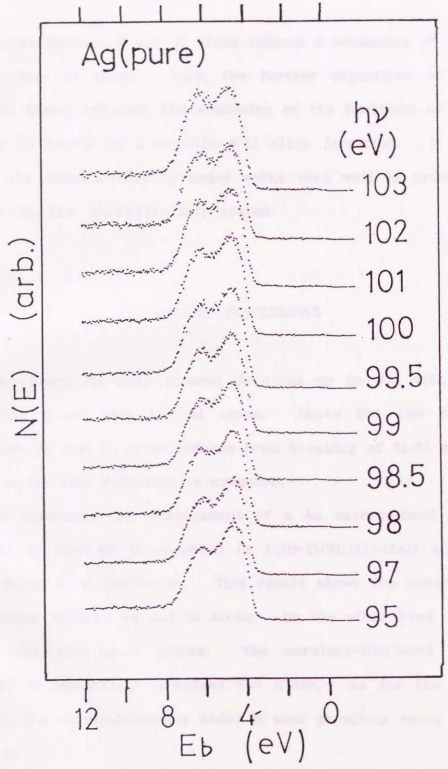

FIG. 11. Valence-band photoemission spectra of pure Ag at photon energies corresponding to those of FIG. 10.

formation between M and Si atoms induces a weakening of the backbond of surface Si atoms. Then, the further deposition of metal atoms beyond $\Theta(M)\sim1$ enhances the weakening of the backbond of substrate Si atoms to result in a metallic M-Si alloy formation. It can be said that the chemical-bonding model works very well in order to explain RTAIF in the Au/Si(111)-(2×1) system.

4.4. CONCLUSIONS

Au atoms lie near topmost Si atoms up to $\Theta\simeq1$ with making non-metallic bonds with the Si atoms. Above $\Theta\simeq1$ the chemical bond between Au and Si atoms induces bond breaking of Si-Si backbonds and the Au-Si alloy formation is promoted.

A resonance-like enhancement of a Au valence-band photoemission signal at $E_b\sim7$ eV is observed in Au($\Theta\sim1$)/Si(111)-(2×1) accompanied by the Si($2p$) core excitation. This result shows the covalent-like-bond formation between Au and Si atoms. On the other hand, it is not the case for the Ag-Si system. The covalent-like-bond formation at $\Theta(M)\leq1$ is essentially important for RTAIF. As for the mechanism of RTAIF, the chemical-bonding model is most promising among the proposed models.

REFERENCES

[1]E. H. Rhoderick and R. H. Williams, *Metal-Semiconductor Contacts*, 2nd ed, (Clarendon Press, Oxford, 1988).

[2]*Thin Films: Interdiffusion and Interactions*, Chem. Soc. Series, edited by J. M. Poate, K. N. Tu, and J. W. Mayer (Wiley, New York, 1978).

[3]L. J. Brillson, Surf. Sci. Rep. 2, 123 (1982).

[4]A. Hiraki, Surf. Sci. Rep. 3, 357 (1983).

[5]W. E. Spicer, T. Kendelewicz, N. Newman, K. K. Chin, and I. Lindau, Surf. Sci. 168, 240 (1986).

[6]A. Hiraki, E. Lugujjo, and J. W. Mayer, J. Appl. Phys. 43, 3643 (1972).

[7]T. Narusawa, S. Komiya, and A. Hiraki, Appl. Phys. Lett. 22, 389 (1973).

[8]the references of Ref. 3 above.

[9]C. Calandra, O. Bisi, and G. Ottaviani, Surf. Sci. Rep. 4, 271 (1984), and references therein

[10]G. Le Lay and J. P. Faurie, Surf. Sci. 69, 295 (1977)

[11]A. Cros, J. Derrien, C. Mouttet, J. P. Gaspard, P. Lambin, and F. Salvan, J. Phys. (Paris) 42, 795 (1980).

[12]E. J. van Loenen, M. Iwami, R. M. Tromp, and J. F. van der Veen, Surf. Sci. 137, 1 (1984), and references therein

[13]G. Le Lay, Surf. Sci. 132, 169 (1983), and references therein

[14]M. Hanbücken and G. Le Lay, Surf. Sci. 168, 122 (1986).

[15]K. Okuno, T. Ito, M. Iwami, and A. Hiraki, Solid State Commun. 34, 493 (1980); K. Okuno, M. Iwami, and A. Hiraki, J. Phys. Soc. Jpn. Suppl. A 49, 1067 (1980).

[16]A. Hiraki, J. Electrochem. Soc, 127, 2662 (1980).

[17]See, for example, J. L. Freeouf, P. S. Ho, and T. S. Kuan, Phys. Rev. Lett. 43, 1836 (1979); and K. N. Tu, Appl. Phys. Lett. 27, 221 (1975).

[18]L. Braicovich, C. M. Garner, P. R. Skeath, C. Y. Su, P. W. Chye, I. Lindau, and W. E. Spicer, Phys. Rev. B 20, 5131 (1979).

[19]G. Rossi, I. Abbati, L. Braicovich, I. Lindau, and W. E. Spicer, Surf. Sci. 112, L756 (1981).

[20]P. H. Barret, R. W. Grant, M. Kaplan, D. A. Keller, and D. A. Shirley, J. Chem. Phys. 39, 1035 (1963).

[21]R. W. Gurney, Phys. Rev. 47, 479 (1935).

[22]J. P. Muscat and D. M. Newns, Prog. Surf. Sci. 9, 1 (1978).

[23]M. Iwami, T. Terada, H. Tochihara, M. Kubota, and Y. Murata, in *Proceedings of the 18th International Conference on the Physics of Semiconductors, Stockholm*, 1986, ed. by O. Engstrom (World Scientific, Singapore, 1987), p.339.

[24]K. L. I. Kobayashi, H. Daimon, and Y. Murata, Phys. Rev. Lett. 50, 1701 (1983).

[25]U. Fano, Phys. Rev. 124, 1866 (1961).

[26]Y. Tezuka, H. Daimon, and S. Ino (unpublished).

[27]K. L. I. Kobayashi, N. Watanabe, H. Nakashima, M. Kubota, H. Daimon, and Y. Murata, Phys. Rev. Lett. 52, 160 (1984).

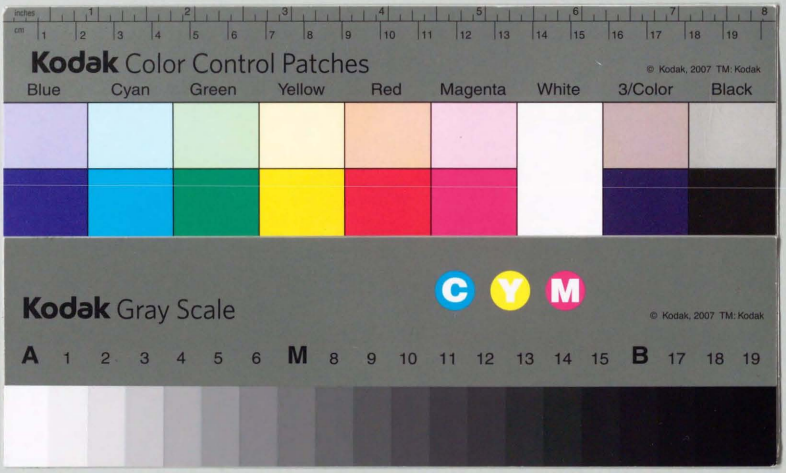
inches
cm
1 2 3 4 5 6 7 8
1 2 3 4 5 6 7 8 9 10 11 12 13 14 15 16 17 18 19
Kodak Color Control Patches
© Kodak, 2007 TM: Kodak
Blue
Cyan
Green
Yellow
Red
Magenta
White
3/Color
Black
Kodak Gray Scale
C
Y
M
© Kodak, 2007 TM: Kodak
A 1 2 3 4 5 6 M 8 9 10 11 12 13 14 15 B 17 18 19